Bone marrow macrophages maintain hematopoietic stem cell (HSC) niches and their depletion mobilizes HSCs

*Ingrid G. Winkler,[1] *Natalie A. Sims,[2] *Allison R. Pettit,[3,4] Valérie Barbier,[1] Bianca Nowlan,[1] Falak Helwani,[1] Ingrid J. Poulton,[2] Nico van Rooijen,[5] Kylie A. Alexander,[3] †Liza J. Raggatt,[3,4] and †Jean-Pierre Lévesque[1,6]

[1]Haematopoietic Stem Cell Laboratory, Mater Medical Research Institute, South Brisbane, Australia; [2]St Vincent's Institute, and Department of Medicine at St Vincent's Hospital, University of Melbourne, Fitzroy, Australia; [3]The University of Queensland Center for Clinical Research, Faculty of Health Sciences, Royal Brisbane Hospital, Herston, Australia; [4]The University of Queensland, Institute for Molecular Bioscience, Brisbane, Australia; [5]Department of Molecular Cell Biology, Vrije Universiteit, Amsterdam, The Netherlands; and [6]University of Queensland, School of Medicine, Brisbane, Australia

In the bone marrow, hematopoietic stem cells (HSCs) reside in specific niches near osteoblast-lineage cells at the endosteum. To investigate the regulation of these endosteal niches, we studied the mobilization of HSCs into the bloodstream in response to granulocyte colony-stimulating factor (G-CSF). We report that G-CSF mobilization rapidly depletes endosteal osteoblasts, leading to suppressed endosteal bone formation and decreased expression of factors required for HSC retention and self-renewal. Importantly, G-CSF administration also depleted a population of trophic endosteal macrophages (osteomacs) that support osteoblast function. Osteomac loss, osteoblast suppression, and HSC mobilization occurred concomitantly, suggesting that osteomac loss could disrupt endosteal niches. Indeed, in vivo depletion of macrophages, in either macrophage Fas-induced apoptosis (Mafia) transgenic mice or by administration of clodronate-loaded liposomes to wild-type mice, recapitulated the: (1) loss of endosteal osteoblasts and (2) marked reduction of HSC-trophic cytokines at the endosteum, with (3) HSC mobilization into the blood, as observed during G-CSF administration. Together, these results establish that bone marrow macrophages are pivotal to maintain the endosteal HSC niche and that the loss of such macrophages leads to the egress of HSCs into the blood. (*Blood*. 2010;116(23):4815-4828)

Introduction

Hematopoietic stem cells (HSCs) reside in bone marrow (BM) and produce all cells required to replenish the blood and immune systems; this process is tightly regulated to maintain a steady number of leukocytes, platelets, and red cells in the blood. Individual HSCs undergo one of several fates: quiescence, apoptosis, cycling either to self-renew, or to generate a more committed hematopoietic progenitor cell (HPC), or migration. These fates are largely controlled by specific local microenvironments (ie, "niches"), in which HSCs and HPCs reside. While HSC niches were conceptualized in the 1970s,[1] it is only in recent years, with the advent of mouse genetic models and live microscopy, that the precise locations and nature of HSC niches have been proposed. Recent microscopy studies have shown that quiescent, long-term, reconstituting HSCs preferentially reside within 20 μm of the interface between compact bone and BM (endosteum) and 10 μm (or 2 cell diameters) from osteoblasts,[2-5] in poorly perfused regions of the BM.[6] Similarly, $Lin^-CD41^-Sca1^+KIT^+CD48^-CD150^+$ HSCs isolated from the femoral endosteal regions have higher long-term reconstitution potential than phenotypically identical HSCs isolated from the central BM.[7] Functional studies support a role for osteoblast-lineage cells to maintain HSCs in the BM in vivo. Transgenic mice with increased osteoblast function have more HSCs in the BM,[8,9] whereas targeted ablation of osteoblasts in vivo results in a progressive loss of HSCs from the BM.[10] Finally, targeted deletion in osteoprogenitors of Dicer-1, necessary for the maturation and processing of all microRNA, results in pancytopenia, exaggerated HSC proliferation, ineffective hematopoiesis, and myelodysplasia.[11] Thus, it appears that the endosteal region and osteoblast-lineage cells provide a unique environment necessary for HSC survival, quiescence, self-renewal, and contribution to long-term hematopoiesis.[11,12]

Despite significant breakthroughs in the identification of cellular and molecular components of BM HSC niches, little is known of how these niches are regulated in vivo. To gain insights in the regulation of endosteal niches, we studied the therapeutic mobilization of HSC. During mobilization, HSPCs (HSCs and HPCs) are forced to migrate and circulate in the blood, allowing the harvest of large numbers of HSCs from patients for transplantation.[13,14] Granulocyte colony-stimulating factor (G-CSF) is the most common mobilizing agent used in the clinic. While inhibition of endosteal osteoblasts has been reported during G-CSF treatment, the mechanisms leading to this inhibition remain unclear.[15-17] While a role of sympathetic nerves innervating the BM and the bone was proposed,[16] recent experiments using transplantation chimeras of wild-type and G-CSF receptor (GCSFR)–deficient mice show that BM leukocytes are also required for osteoblast suppression and HSPC mobilization by G-CSF.[17]

We confirm that G-CSF rapidly and transiently ablates endosteal osteoblasts[17] and extend these observations by demonstrating a cessation of endosteal bone formation. Strikingly, this

Submitted November 10, 2009; accepted August 7, 2010. Prepublished online as *Blood* First Edition paper, August 16, 2010; DOI 10.1182/blood-2009-11-253534.

*I.G.W., N.A.S., and A.R.P. contributed equally to this work.

†L.J.R. and J.-P.L. contributed equally to this work.

The online version of this article contains a data supplement.

The publication costs of this article were defrayed in part by page charge payment. Therefore, and solely to indicate this fact, this article is hereby marked "advertisement" in accordance with 18 USC section 1734.

Table 1. Primers and probes used in qRT-PCR analyses

	Primers and probes
Osteocalcin	Forward (32f) 5′-TTCTGCTCACTCTGCTGACCCT-3′
	Reverse (137b) 5′-CCCTCCTGCTTGGACATGAA-3′
Osterix	Forward (126f) 5′-AGCTCACTATGGCTCCAGTCC-3′
	Reverse (245b) 5′-GCGTATGGCTTCTTTGTGCCT-3′
CXCL12	Forward (198f) 5′-GAGCCAACGTCAAGCATCTG-3′
	Reverse (298b) 5′-CGGGTCAATGCACACTTGTC-3′
KL	Forward (80f) 5′-GCTACCCAATGCTGGGACTA-3′
	Reverse (286b) 5′-CCGCAGATCTCCTTGGTTT-3′
Angiopoietin-1	Forward (1645f) 5′-CAAATGCGCTCTCATGCTAA-3′
	Reverse (1806b) 5′-ATGGTGGTGGAACGTAAGGA-3′
VE-cadherin	Forward (722f) 5′-CGTGGTGGAAACACAAGATG-3′
	Reverse (902b) 5′-TGGGTCCACAACAGTCAGAA-3′
Fibronectin	Forward (51f) 5′-GTCAGTCAAAGCAAGCCCGG-3′
	Reverse (288b) 5′-CAGTCCCAGATCATGGAGTC-3′
Runx2	Forward (904f) 5′-CCAAGAAGGCACAGACAGAA-3′
	Reverse (995b) 5′-ATACTGGGATGAGGAATGCG-3′
	Probe(949b)FAM-5′-CCCTAAATCACTGAGGCGATCAGAGAA-3′-BHQ1
PTHR1	Forward(894f) 5′-GATTCTGGTGGAGGGACTGT
	Reverse(1090b) 5′-GGATGATCCACTTCTTGTGC-3′
	Probe(1039b)FAM-5′-TCCCAGCACCCAGTGTTGGC-3′-BHQ1
β2-microglobulin	Forward 5′-CTGGTCTTTCTGGTGCTTGTC-3′
	Reverse 5′-GTATGTTCGGCTTCCCATTC-3′
	probe(94f)FAM-5′-CACTGACCGGCCTGTATGCTATCCA-3′-BHQ1

depletion of endosteal osteoblasts and bone formation was accompanied by a loss of BM macrophages, particularly osteoblast-supportive endosteal macrophages (osteomacs). Furthermore, depletion of BM macrophages, in particular, a novel $CD11b^+F4/80^+Ly6\text{-}G^+$ phagocytic macrophage population, in 2 mechanistically unrelated in vivo models, was sufficient to suppress endosteal osteoblasts, inhibit the expression of HSC-supportive cytokines at the endosteum, and elicit HSPC mobilization into the peripheral blood. This study reveals a critical role for BM macrophages in maintaining the endosteal HSC niche.

Methods

Procedures were approved by the University of Queensland Animal Experimentation Ethics Committee.

G-CSF mobilization

Dipeptidylpeptidase-1 (*DPP-1*) and *GCSFR* knockout mice backcrossed into C57BL/6 were kindly provided by Drs C. Pham and D. C. Link (Washington University, St Louis, MO). All experiments were performed on 12- to 14-week-old skeletally mature C57BL/6 mice, except G-CSF–treated control mice for protease concentration assays (see Figure 7A), which were 129Sv. To assess the effects of G-CSF mobilization, mice were injected twice daily subcutaneously with 125-μg/kg injections of recombinant human G-CSF (a kind gift of Amgen) or saline for up to 6 consecutive days. When required, osteoclast activity was blocked by a 6-day treatment with 20-μg/kg/d subcutaneous injections of zoledronate (Zometa; Novartis Pharmaceuticals) before sacrifice, and G-CSF was administered twice subcutaneously at 125 μg/kg for the last 3 days before sacrifice.

To assess bone formation during mobilization, G-CSF or saline was injected from days 0 to 5 as described above. Calcein (Sigma-Aldrich) was injected intraperitoneally at a dose of 20 mg/kg on days 1 and 7. Xylenol orange (Sigma-Aldrich) was injected intraperitoneally at a dose of 200 mg/kg on days 4 and 10. Mice were killed on day 12.

Macrophage depletion in vivo

In a first model, myeloid cells were depleted from skeletally mature macrophage-Fas-induced apoptosis (Mafia) transgenic mice by daily intravenous retro-orbital injection of 10 mg/kg/d AP20817 ligand (generous gift from ARIAD Pharmaceuticals; www.ariad.com/regulationkits) dissolved in 4% ethanol, 10% polyethylene glycol 400, and 1.7% Tween-20.[18] Controls were Mafia mice injected with vehicle alone and wild-type mice injected with AP20817 ligand.

In a second model, clodronate (dichloromethylene bisphosphonate), a gift from Roche Diagnostics, was packaged into liposomes as previously described.[19] Empty liposomes were prepared in the same conditions in phosphate-buffered saline (PBS) without clodronate. Phagocytic macrophages were depleted in vivo by retro-orbitally, injecting 250 μL/25 g clodronate-loaded liposome suspension every second day. Control mice were injected with an equivalent volume of saline or PBS-loaded liposomes.

Tissue harvesting and RNA extraction

At specified time points, mice were anesthetized and 1 mL of blood was collected into heparinized tubes by cardiac exsanguinations. Red cells were lysed from blood as previously described.[20] Spleens were harvested, weighed, and dissociated in PBS with 2% fetal calf serum. Cells and RNA from enriched central BM, and endosteal RNA were isolated from femurs as previously described.[21] Tibias were fixed in PBS containing 4% paraformaldehyde overnight at 4°C and stored in 70% ethanol until embedding in methacrylate[22] for undecalcified bone histomorphometry, or decalcified in 14% EDTA (ethylenediaminetetraacetic acid) and embedded in paraffin for immunohistochemistry and enzyme staining.

qRT-PCR

RNA was extracted with TRIzol, precipitated, DNase treated, and reverse transcribed using random hexamers. Quantitative real-time reverse transcription polymerase chain reaction (qRT-PCR) with SYBR green for osteocalcein, osterix, Kit-ligand (KL), angiopoietin-1 (Ang-1), vascular endothelial (VE)–cadherin, and fibronectin or using TaqMan probes (labeled 5′ with 6-carboxyfluorescein [FAM] and 3′ with blackhole quencher-1 [BHQ-1]) for Runx2 and parathyroid hormone receptor 1 (PTHR1) were performed following the manufacturer's instructions (Applied Biosystems). Oligonucleotide sequences are shown in Table 1. Primers were designed to cross intron-exon boundaries to not amplify genomic DNA, with the exception of osterix that is encoded by a single exon. A PCR from each sample before reverse transcription confirmed the absence of genomic DNA. RNA levels were standardized by parallel qRT-PCR using primers to the housekeeping gene, β2-microglobulin.

Histomorphometry

Tibial samples were embedded in methacrylate, undecalcified 5-μm sections were stained with toluidine blue, and histomorphometry carried out in the trabecular bone of the proximal tibial secondary spongiosa using the Osteomeasure system (OsteoMetrics).[22] For mineral appositional rates, sections remained unstained and fluorochromes were visualized by epifluorescence microscopy.[22]

Calcein and xylenol orange mineralization fronts were visualized on a Zeiss LSM 510 Meta confocal laser-scanning microscope. Calcein fluorescence was excited at 488 nm, with an Ar laser and emission detected through a 505-530-nm filter, whereas xylenol orange fluorescence was excited at 543 nm with a He-Ne laser and emission was detected through a 560-nm filter. Each fluorophore was excited, scanned, and acquired separately.

Cell counts and colony assays

Leukocytes were counted on a Sysmex KX-21 automated cell counter. For myeloid colony assays, cells were deposited in 35-mm Petri dishes and covered with 1 mL of Iscove modified Dulbecco medium supplemented with 1.6% methylcellulose (high-viscosity Methocell MC; Fluka), and 35% fetal calf serum. Optimal concentrations of mouse interleukin-3 (IL-3), IL-6, and soluble KL were added as conditioned media from stably transfected baby hamster kidney (BHK) cell lines. Colonies were counted after 10 days of culture.

Competitive repopulation assays

The content of mobilized blood samples in competitive repopulating HSCs was determined in competitive repopulation assays. The day before blood harvest, recipient congenic B6.SJL CD45.1$^+$ mice were lethally irradiated with 11.0 Gy in 2 split doses 3 hours apart. Then, 50-μL blood samples from 4 mobilized CD45.2$^+$ C57BL/6 mice were pooled within each treatment group, and 50-μL blood aliquots were taken from this pool and mixed with 200 000 competitive whole BM cells from untreated B6.SJL CD45.1$^+$ mice in a total volume of 200 μL and injected retro-orbitally into each lethally irradiated recipient. Recipients were maintained with antibiotics for the first 3 weeks posttransplantation and tail bled 16 weeks posttransplantation to determine CD45.2 (test donor blood) versus CD45.1 (competitive whole BM cells) in myeloid, B, and T lineages by flow cytometry using CD45.1-phycoerythrin (PE), CD45.2-fluorescein isothiocyanate (FITC), B220-allophycocyanin (APC)–cyanin (CY) 7, CD11b-PECY7, CD3-biotin, and streptavidin (SAV)–Pacific Blue (PB).

Flow cytometry

After flushing with PBS, enriched central BM cells were pelleted at 370*g* for 5 minutes at 4°C and resuspended in CD16/CD32 hybridoma 2.4G2 supernatant to block immunoglobulin G Fc (IgGFc) receptors, except for myeloid progenitor stains.

HSCs were stained with the biotinylated lineage antibody cocktail (CD3, CD5, B220, CD11b, Gr-1, and Ter119) and biotinylated CD41 together with SAV-PB, Sca-1-PECY7, KIT-APC, CD48-FITC, and CD150-PE.

Mature myeloid cells were stained with CD11b-PECY7, antilymphocyte (LY)-6G-PE (clone 1A8), and anti-F4/80-Alexa Fluor 647.

Osteoblast-lineage cells, multipotent stromal cells (MSCs), and endothelial cells were isolated from the endosteum following collagenase digestion of cleaned bone fragments as previously described.[6,23-25] Hematopoietic cells were removed by magnetic depletion using biotinylated lineage antibodies (CD3, CD5, B220, CD11b, Gr-1, and Ter119), followed by depletion with MACS beads conjugated to SAV (Miltenyi Biotec). Cells were then stained at 4°C with CD45-APCCy7, CD31-APC, CD51-PE, stem-cell antigen 1 (Sca-1)–PECY7, and SAV-FITC for wild-type mice or SAV-PB for col2.3Cre$^+$R26R-YFP$^{+/+}$ mice and sorted on the following gating strategy: CD45$^-$Lin$^-$CD31^{bright} endothelial cells; CD45$^-$Lin$^-$CD31$^-$Sca-1^{bright}CD51$^+$ MSC; and CD45$^-$Lin$^-$CD31$^-$Sca-1$^-$CD51$^+$ osteoblast lineage cells.[6,23-25]

All antibodies were from BD Pharmingen, except CD150-PE (clone TC15-12F12.2) and anti-F4/80-AlexaFluor647 (clone CI:A3-1), which were from Biolegend. Data were acquired on LSRII (BD Biosciences) or CyAn (Dako Cytomation) flow cytometers and analyzed following compensation with single-color controls using FlowJo Version 8.8.6 software (Tree Star).

Immunohistochemistry and TRAP enzyme histology

Fixed and decalcified hind limb bones were embedded in paraffin and 5 μm sections cut and placed on SuperFrost Plus slides (Menzel). Sections were deparaffinized and rehydrated with xylene and graded ethanol and washed in tris(hydroxymethyl)aminomethane-buffered saline (TBS) (immunohistochemistry) or deionized water (histology). F4/80 (rat anti-mouse F4/80; AbD Serotec) and osteocalcin (rabbit anti–mouse; Alexis Biochemicals) immunohistochemical staining was carried out as previously described.[26] Specificity of staining was confirmed by comparison to serial sections stained with matched isotype control antibodies (rat IgG2b; AbD Serotec and normal rabbit IgG; Santa Cruz Biotechnology, respectively). Tartrate-resistant acid phosphatase (TRAP) staining was performed as previously described.[27] All sections were examined using a Nikon Eclipse 80i microscope with a Nikon D5-Ri1 camera and NIS-elements BR 3.0 imaging software.

Protease concentration

Quantification of active neutrophil elastase (NE) and cathepsin (catG) BM fluids using specific chromogenic substrates, and gelatin zymopgraphy to measure matrix metalloproteinase-9 (MMP-9), was carried out as previously described.[28,29]

Statistical analysis

Significance levels were calculated using the Student *t* test for colony assays, flow cytometric analyses, and qRT-PCR, or 2-way analysis of variance followed by Fisher protected least significant difference post-hoc test for histomorphometric measurements.

Results

HSPC mobilization by G-CSF inhibits endosteal niches for HSCs

Administration of G-CSF to skeletally mature mice increased the number of hematopoietic colony-forming cells (CFCs) and long-term reconstituting Lin$^-$CD41$^-$Sca1$^+$KIT$^+$CD48$^-$CD150$^+$ HSCs[30] in the blood from day 2 of G-CSF administration (Figure 1A), reaching a plateau between days 4 and 6, and rapidly returned to baseline when G-CSF administration was ceased (Figure 1A). Endosteal markers of bone formation, including the proportion of bone surface lined with osteoblasts (ObS/BS) or newly formed bone matrix (osteoid, OS/BS), all decreased by 16- to 18-fold during mobilization, but rebounded 4 days after cessation of G-CSF administration to 2-fold above baseline (Figure 1B), then continued to decrease until day 21. Both ObS/BS and OS/BS dropped 40%-50% on day 1 and 75% on day 2 of G-CSF administration, whereas the number of circulating CFCs and Lin$^-$Sca1$^+$KIT$^+$ and long-term reconstituting Lin$^-$CD41$^-$Sca1$^+$KIT$^+$CD48$^-$CD150$^+$ HSCs significantly increased in the blood only on day 2.

Messenger RNA for osteoblast lineage–specific genes, including osteocalcin, Runx2/Cbfa1, and osterix,[31,32] were also reduced during G-CSF treatment (supplemental Figure 1, available on the *Blood* Web site; see the Supplemental Materials link at the top of the online article). Osteocalcin mRNA decreased 50-fold, returning to basal levels 4 days following cessation of G-CSF, paralleling the

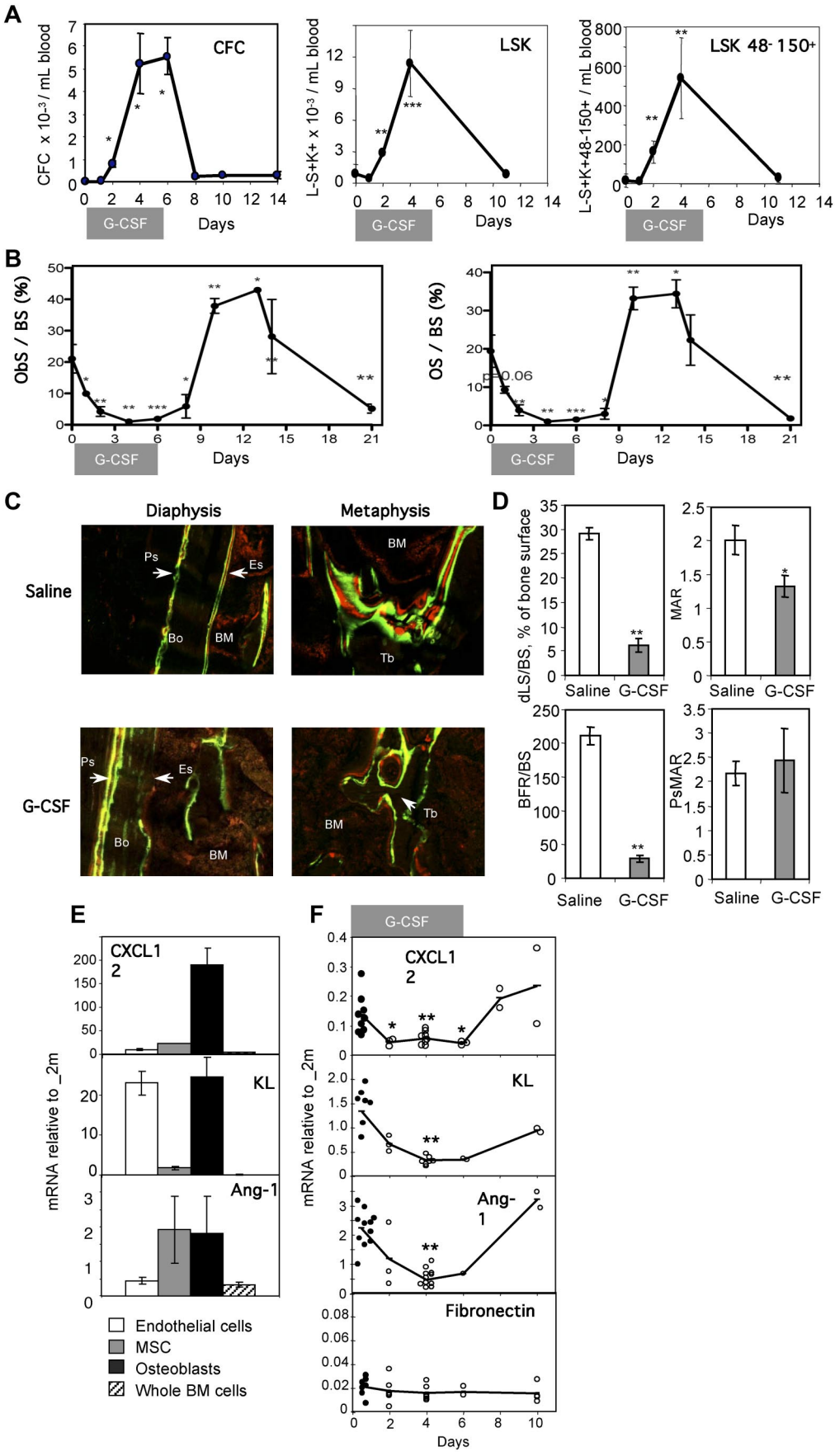

Figure 1. Impaired endosteal bone formation and HSC niche function in G-CSF–mobilized mice. (A) Mobilization of CFCs, $Lin^-Sca1^+KIT^+$ (LSK) HSPCs, and $Lin^-CD41^-Sca1^+KIT^+CD48^-CD150^+$ phenotypic HSCs in blood following G-CSF administration. Data are means ± SD of 4 mice per group. (B) Histomorphometry for osteoblast surface per unit of bone surface (ObS/BS) and osteoid surface per bone surface (OS/BS) in the trabeculae of the proximal tibial secondary spongiosa from mice mobilized for 6 days with G-CSF. Data are mean ± SEM of both tibias from 3-6 mice per group from one representative experiment of 2 independent experiments. (C) Dynamic histomorphometry in mice mobilized with G-CSF. Mice treated with saline or G-CSF for 6 days were injected every third day alternatively with either calcein or xylenol orange and killed at day 12. Tibial sections were analyzed by confocal laser-scanning micrographs (×20). Green and red lines are areas of bone that mineralized and incorporated calcein and xylenol orange, respectively. BM is slightly red due to nonspecific incorporation of xylenol orange by BM cells, whereas solid bone is dark, except where labeled. Top micrographs are across the cortical bone on the anterofibular side, whereas bottom micrographs are across the secondary spongiosa of the metaphysis. (D) The incorporation of calcein lines was quantified in the secondary spongiosa and at the periosteum; shown are percentage of trabecular bone surface covered by double-calcein lines (dLS/BS), trabecular mineral appositional rate (MAR) between double-calcein lines, trabecular bone forming rate corrected for bone surface (BFR/BS), and periosteal mineral appositional (PsMAR). (E) Expression levels of CXCL-12, KL, and Ang-1 mRNA in endothelial cells (□), mesenchymal stromal cells (▨) and osteoblasts (■) sorted from nonmobilized endosteum, and whole BM cells (▨). All expression levels are relative to β2-microglobulin mRNA and are the average of 2 experiments in which populations were sorted from 10 mice each. (F) mRNA for CXCL-12, KL, Ang-1, and fibronectin were quantified at the indicated time points of G-CSF-mobilization by qRT-PCR. All expression levels are relative to β2-microglobulin mRNA. Each symbol represents the result from an individual mouse. Data are means ± SD . $^{***}P < .001$, $^{**}P < .01$, and $^{*}P < .05$.

changes in ObS/BS and OS/BS. In addition, mRNA levels for PTHR1, the receptor for both parathyroid hormone (PTH) and PTH-related protein, which is expressed by osteoblasts, were also decreased by 24-fold by G-CSF treatment.

To confirm a functional alteration in bone formation, labeling with the fluorescent calcium chelators, calcein and xylenol orange, was carried out during G-CSF treatment and recovery. These labels rapidly incorporate into bone, being mineralized at the time of injection (Figure 1C). Continuous bone formation results in labeling of the bone surface, with 2 lines of calcein (green) alternating with 2 lines of xylenol orange. Both mineralization and bone formation were strongly reduced on both endocortical (diaphysis) and trabecular surfaces (metaphysis) in G-CSF–mobilized mice, compared with controls. In contrast, the outer cortical surface (periosteum) was labeled with well-separated multiple fluorochromes in both G-CSF–treated mice and controls, indicating that the disruption in bone formation induced by G-CSF treatment was restricted to the endosteum (ie, surfaces in contact with BM). Quantification of calcein labels (Figure 1D) revealed that the percentage of bone surfaces on which bone formation occurred (double calcein-labeled bone surface dLS/BS) was significantly reduced by G-CSF treatment from 29% ± 1% to 6% ± 2%. On those few surfaces on which bone formation occurred during mobilization, the mineral apposition rate (MAR) was reduced by 30%. Together, the endosteal trabecular bone formation rate per unit bone surface (BFR/BS) was reduced by 90% in G-CSF–mobilized mice. In contrast, periosteal mineralization surface (PsMAR) was not affected by G-CSF administration. This confirms that only mineralization by osteoblasts in direct contact with the BM is inhibited during HSPC mobilization.

HSCs are supported by cytokines and chemokines produced within specific niches at the endosteum, including KL, Ang-1, and CXCL12. To determine whether these cytokines were expressed by osteoblasts, we sorted endosteal cells into: (1) $CD45^-Lin^-CD31^{bright}$ endothelial cells, (2) $CD45^-Lin^-CD31^-Sca\text{-}1^{bright}CD51^+$ MSCs with osteogenic, chondrogenic, and adipogenic potential,[24,25] and (3) $CD45^-Lin^-CD31^-Sca\text{-}1^-CD51^+$ osteoblast lineage cells.[6,23,24] qRT-PCR for osteocalcin and the endothelial cell marker VE-cadherin validated this sorting strategy (supplemental Figure 2). This strategy was further validated by analyzing these 3 populations from $col2.3Cre^+$ $R26R\text{-}YFP^{+/+}$ mice, in which a Cre-inducible yellow fluorescent protein (YFP) reporter was activated only in maturing and mature osteoblasts.[33] In these mice, 38% ± 13% of cells (n = 3 mice) in the osteoblast gate were YFP^+, while only 5% ± 1% of cells in the MSC gate were YFP^+, and YFP^+ cells were undetectable in the endothelial gate (supplemental Figure 2).

We then evaluated expression of CXCL12, KL, and Ang-1 in endothelial cells, MSCs, and osteoblast lineage cells by qRT-PCR (Figure 1E). CXCL12, a chemokine necessary for HSPC retention in the BM[34,35] and HSC survival and proliferation,[36] was expressed at high levels by osteoblast lineage cells and at much lower levels by MSCs and endothelial cells. Ang-1, a cytokine essential to HSC development,[2] was also transcribed by both osteoblast lineage cells and MSCs. Finally, KL, a cytokine that acts on all hematopoietic progenitors and HSCs, was transcribed by both osteoblast lineage and endothelial cells. These mRNAs were all expressed at much higher levels in endosteal cells, compared with the whole BM population (Figure 1E). Importantly, during G-CSF administration, mRNA levels of CXCL12, KL, and Ang-1 were all significantly decreased at the endosteum (Figure 1F). In contrast, expression of fibronectin, an extracellular matrix protein produced by BM stromal cells, remained unaltered. Taken together, these observations demonstrate that the expression of HSC-trophic cytokines are decreased within the endosteum during mobilization, suggesting impaired niche function.

HSPC mobilization is not mediated by osteoclasts

To determine whether osteoclasts were involved in the HSC mobilization and osteoblast inhibition, histochemical staining for TRAP and histomorphometry of trabecular bone both showed that the number of osteoclasts on endosteal surfaces (NOc/BPm) was not significantly altered during G-CSF administration (Figure 2A-B). mRNA for cathepsin K, a marker of active osteoclasts, increased by 10-fold, but only 4 days after the cessation of G-CSF administration (Figure 2C), indicating that any increase in osteoclast number or activity occurs only after HSPC mobilization has ceased. The loss of mature osteoblasts during G-CSF treatment and egress of HSPC to the blood is therefore unlikely to be dependent on osteoclast depletion; in fact, the normal coupling between osteoclast and osteoblast numbers appears to be disrupted during G-CSF administration.

To confirm whether osteoclasts are necessary for G-CSF–induced mobilization of HSPC, osteoclasts were inhibited with zoledronate[37,38] before and during G-CSF mobilization. As expected, zoledronate treatment dramatically decreased endosteal osteoclast numbers and did not prevent the reduction in osteoblast numbers in G-CSF–mobilized mice (Figure 2D-E). Mice treated with zoledronate and G-CSF showed enhanced mobilization of CFC into the blood and spleen, compared with mice mobilized with G-CSF alone (Figure 2F-G), which was accompanied by a greater reduction in ObS/BS (Figure 2E). Zoledronate alone did not induce mobilization (not shown). To determine whether repopulating HSPCs were also mobilized, we performed competitive repopulation assays with the mobilized blood samples. Blood from individual C57BL/6 $CD45.2^+$ mice were pooled in equal volume within each treatment group, and 50 μL of pooled blood was mixed with 200 000 competing BM cells from untreated congenic $CD45.1^+$ mice and transplanted into lethally irradiated $CD45.1^+$ hosts. After transplant, zoledronate significantly increased multilineage chimerism from mobilized $CD45.2^+$ blood HSCs (Figure 2H). Taken together, our data confirm that osteoclasts are not required for HSPC mobilization or the osteoblast suppression associated with mobilization.

G-CSF mobilization disrupts endosteal osteomac and BM macrophage distribution

$F4/80^+$ osteomacs reside in osteal tissues and are intercalated and/or associated with other bone-lining cells.[26] These osteomacs form a canopy over mature osteoblasts at sites of bone formation (Figure 3B), support osteoblast function in vitro, and are required for the maintenance of osteoblasts in vivo.[26] Since macrophages,[39] but not osteoblasts,[16,23] express GCSFR, osteomacs were investigated as a candidate mediator of G-CSF effects on osteoblasts. We found that $F4/80^+$ osteomacs were reduced on endosteal surfaces from day 2 of G-CSF administration (Figure 3C). This reduction was accompanied by a clustering of $F4/80^+$ cells in the central BM, particularly around endothelial sinuses. Between days 4 and 6 of mobilization, $F4/80^+$ cells at the endosteum were virtually undetectable (Figure 3D).

$F4/80^+$ cells within the endosteal region were detected again 2 days after the cessation of G-CSF administration (Figure 3E). The

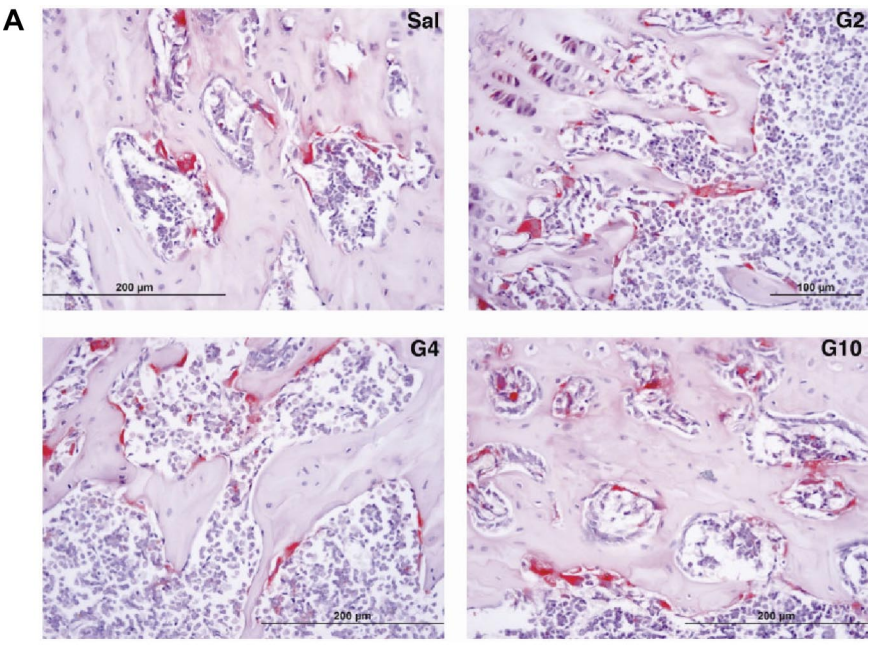

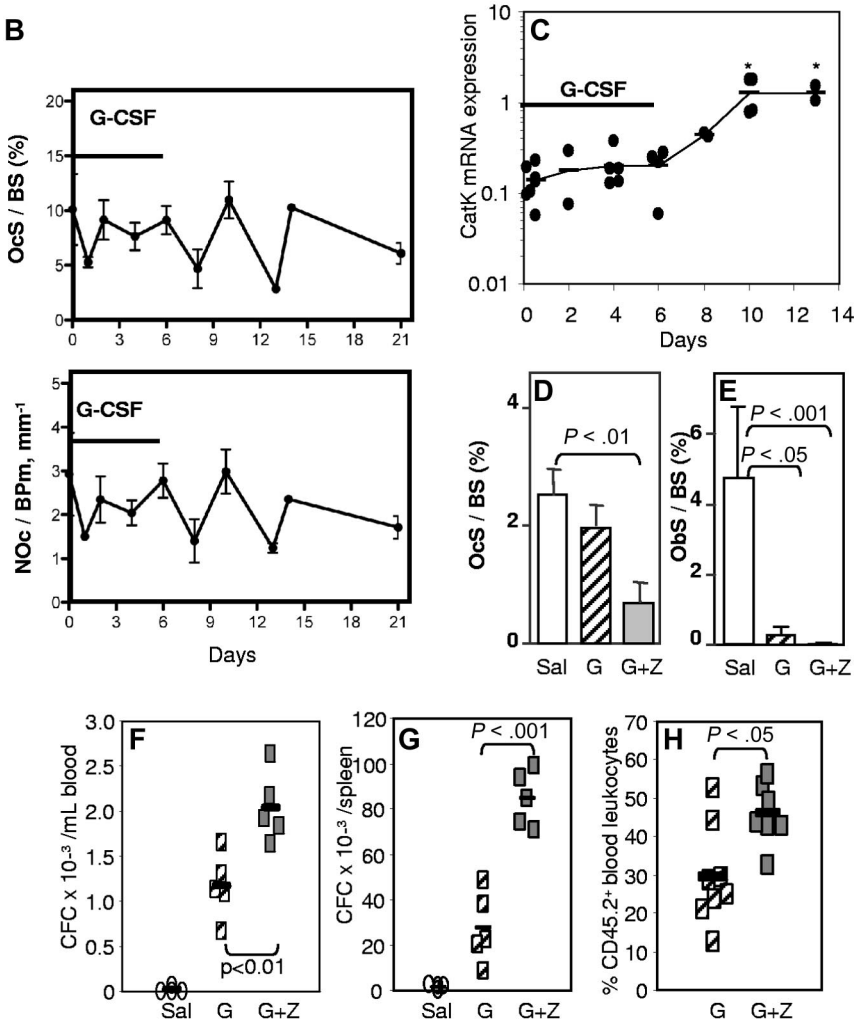

Figure 2. G-CSF–induced mobilization is not mediated by osteoclasts. (A) TRAP staining in tibial spongiosa from mice treated with saline (Sal) or G-CSF for 2 (G2), 4 (G4), or 6 days, followed by 4 days of recovery (G10). Osteoclasts are stained in red. (B) Histomorphometry for osteoclast surface per bone surface (OcS/BS) and number of osteoclasts per bone perimeter (NOc/BPm) in the trabeculae of the proximal tibial secondary spongiosa from mice mobilized for 6 days with G-CSF. (C) qRT-PCR for cathepsin K mRNA in endosteal cells. $^*P < .05$. (D-F) Effect of zoledronic acid and G-CSF treatment on osteoclast (D) and osteoblast (E) surface per bone surface in the trabeculae, mobilization of CFCs into blood (F) and spleen (G), and mobilization of competitive repopulating cells (H). In panels B, D, and E, each bar is mean ± SEM of 4 mice per group. In panels C and F through H, each symbol represents an individual mouse, and bars are the mean from one representative experiment of 2 independent experiments.

osteomac canopy over cuboidal osteoblasts on endosteal surfaces was fully restored by day 10 (Figure 3F). Thus, the kinetics of osteomac loss parallels the loss of endosteal osteoblasts in the same animals (Figure 1).

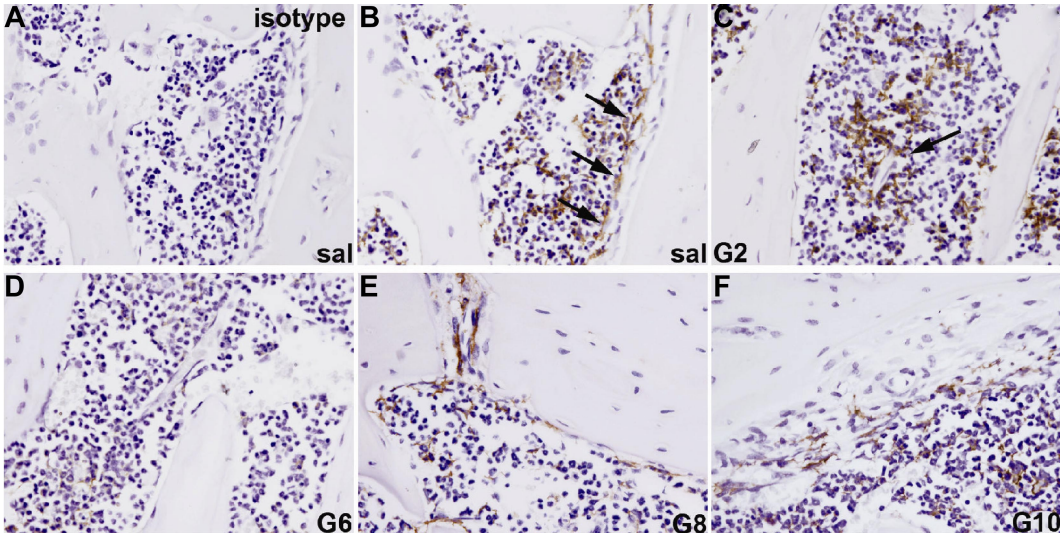

Figure 3. Loss of osteomacs from endosteal surface during G-CSF–induced mobilization. Bone sections from mice treated with saline (A,B) or G-CSF for 2 (C), 6 (D), or for 6 days with G-CSF, followed by a recovery of 2 (E) or 4 days (F), were stained with a monoclonal antibody against the F4/80 antigen (B-F) or an isotype-matched nonimmune antibody (A). F4/80$^+$ cells are stained brown. F4/80$^+$ osteomacs forming a canopy over active osteoblasts at endosteal surfaces were detected in saline-treated animals (B, arrows) as well as 4 days following cessation of a 6-day G-CSF treatment (F). Clustering of F4/80$^+$ cells around blood vessels was observed after 2 days of treatment (C, arrows). Pictures are representive of 1 mouse of 3 mice per time point.

In vivo depletion of myeloid cells in Mafia transgenic mice deregulates endosteal niches and mobilizes HSPC

To determine the contribution of BM and endosteal macrophages to the regulation of endosteal niches, we ablated *c-fms*–expressing cells, which include most mature myeloid cells, such as macrophages and granulocytes, in Mafia transgenic mice. In these mice, a *c-fms* promoter induces the expression of a transgene containing green fluorescent protein (GFP) and a suicide fusion protein made of the FK506-binding protein and the cytoplasmic domain of Fas. Systemic administration of AP20187 dimerizes the suicide protein to cause Fas-mediated apoptosis in *c-fms*–expressing cells.[18] Cells expressing the transgene GFP were assessed in Mafia mouse BM by flow cytometry (Table 2). As expected, more than 85% of BM F4/80$^+$Ly-6G$^-$CD11b$^+$ macrophages and 90% of Ly-6G$^+$F4/80$^-$CD11b$^+$ granulocytes were GFP$^+$, indicating the expression of the Mafia suicide transgene in both cell populations. Importantly, the Mafia transgene was not expressed in osteoblast lineage cells, MSCs, or BM endothelial cells.

Administration of AP20187 ligand ablated transgene-expressing GFP$^+$CD11b$^+$ myeloid cells, Ly-6G$^+$ granulocytes, and F4/80$^+$ macrophages in the BM (Figure 4A,B,F) as previously reported.[18] In addition, AP20187 treatment elicited robust CFC mobilization into the blood and spleen (Figure 4C-D). qRT-PCR analyses on endosteal RNA from treated Mafia mice revealed a 35-fold decrease in osteocalcin, an 8-fold decrease in Ang-1, and a 3-fold decrease in KL mRNA (Figure 4E), demonstrating impairment of endosteal HSC niches following ligand treatment. Immunohistochemistry showed a depletion of BM macrophages and osteomacs on metaphyseal and diaphyseal surfaces in AP20187-treated Mafia mice (Figure 4F) and an almost complete loss of osteocalcin-positive osteoblasts from trabecular and endocortical bone surfaces (Figure 4F). Osteoclasts, as assessed by TRAP staining, were moderately decreased at day 5 (data not shown). None of these effects were observed in wild-type mice treated with AP20187 ligand (Figure 4A-F), demonstrating that this drug is not toxic for myeloid cells, HSPC, or mature osteoblasts in the absence of the Mafia transgene. These results suggest that macrophage depletion alone is sufficient to alter endosteal HSC niches and lead to HSC mobilization into the blood.

Table 2. GFP expression in stromal cells, myeloid cells, HPCs, and stem cells from Mafia mice

Cell types	Phenotypes	% GFP$^+$ cells
Myeloid cells	CD11b$^+$	88.4 ± 0.7
Granulocytes	CD11b+ F4/80$^-$Ly-6G$^+$	96.9 ± 0.3
Macrophages	CD11b$^+$ F4/80$^+$Ly-6G$^-$	85.5 ± 1.7
	CD11b$^+$ F4/80$^+$ Ly-6G$^+$	88.6 ± 0.7
Endothelial cells	Lin$^-$CD45$^-$CD31$^+$	0.1 ± 0.1
MSCs	Lin$^-$CD45$^-$CD31$^-$Sca1$^+$	0.0 ± 0.0
Osteoblasts	Lin$^-$CD45$^-$CD31$^-$Sca1$^-$CD51$^+$	0.6 ± 0.1

Data are average ± SD of 3 mice. Wild-type mice had no cells (< 0.05%) expressing GFP.

In vivo depletion of phagocytes with clodronate-loaded liposomes disrupts endosteal niches and mobilizes HSPC

The mafia mouse model is not ideal as G-CSF concentration increases in blood during depletion and other myeloid cells are depleted, in addition to macrophages. Our data were confirmed in a second mechanistically unrelated model of macrophage depletion in vivo. Mice were injected intravenously with clodronate-loaded liposomes (clo-lip), control PBS-loaded liposomes (PBS-lip), or saline for 1-4 days. Clo-lip treatment (but not PBS-lip) specifically kills phagocytes, the only cells capable of engulfing liposomes.[19,40] Although BM contains multiple monocyte/macrophage/granulocyte populations, only some were depleted following Clo-lip administration. Specifically, a macrophage population with the unusual F4/80$^+$Ly-6G$^+$CD11b$^+$ phenotype was reduced by 95% within 24 hours of clo-lip administration and remained depleted throughout clo-lip treatment (Figure 5A). Interestingly, BM granulocytes (Ly-6G$^+$F4/80$^-$CD11b$^+$) were not affected by clo-lip administration until later time points (4 days), when their numbers eventually increased by 2.5-fold above baseline. As a control, BM T-cell numbers remained unaltered during clo-lip administration (not shown).

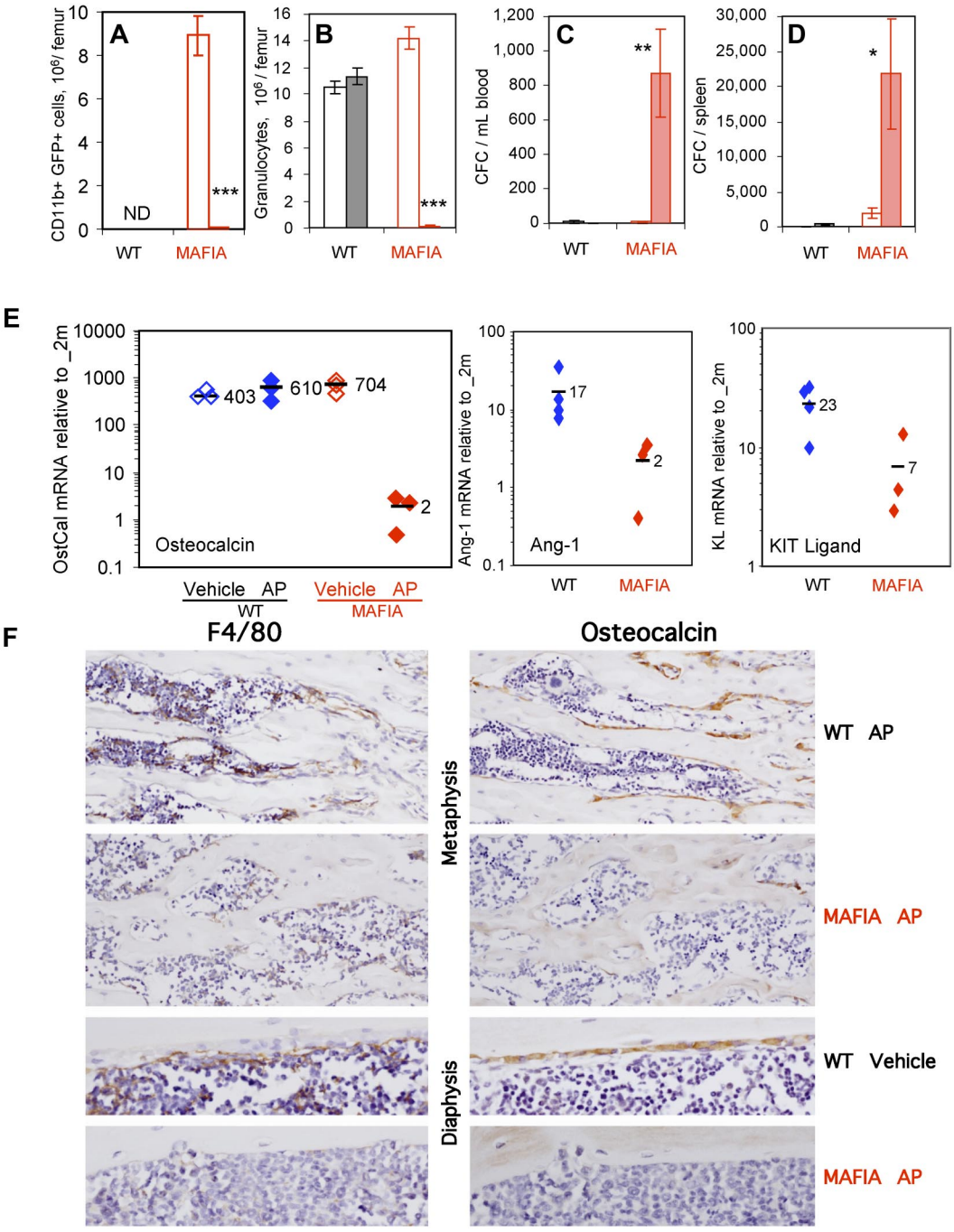

Figure 4. In vivo depletion of myeloid cells in Mafia mice results in HSPC mobilization and collapse of endosteal niches. Effect of a 5-day systemic treatment with AP20187 ligand (filled columns) or vehicle (empty columns) in Mafia and wild-type mice on femoral content in $CD11b^+GFP^+$ myeloid cells (A) and $CD11b^+Ly6\text{-}G^+$ granulocytes (B) and number of CFCs mobilized into blood (C) and spleen (D). $CD11b^+GFP^+$ myeloid cells were not determined (ND) in wild-type mice, as they do not express the GFP transgene. Data are mean ± SD of 4-6 mice per group. $^{***}P < .001$, $^{**}P < .01$, and $^{*}P < .05$ between vehicle- and AP20187-treated mice. (E) Effect of a 5-day systemic treatment with AP20187 ligand (filled symbols) or vehicle (empty columns) in Mafia and wild-type mice on osteocalcin, Ang-1, and KL in endosteal cells measured by qRT-PCR. Each symbol represents an individual mouse; bars are means. (F) Immunohistochemical staining of tibial sections from Mafia and C57BL/6 mice treated for 5 days with AP20187 or vehicle. Brown positive staining for F4/80 (left panels) or osteocalcin (right panels) is shown in near serial section of metaphyseal and diaphyseal endocortical regions. $F4/80^+$ osteomacs can be seen directly on bone surfaces or immediately adjacent to cubiodal $osteocalcin^+$ osteoblasts in control groups, and osteomac canopy structure is clearly evident on endocortical bone. Dramatic depletion of $F4/80^+$ cells and subsequent loss of $osteocalcin^+$ osteoblasts is clearly evident in ligand-treated Mafia mice. Original magnifications ×20 and ×40. All sections were counterstained with hematoxylin.

Depletion of phagocytic macrophages in the BM by clo-lip administration elicited a significant mobilization of CFCs and phenotypic $Lin^-Sca1^+KIT^+$ HSPCs within 24 hours (Figure 5B). While no long-term competitive repopulating HSCs capable of multilineage engraftment were detected in the blood of control PBS-lip–injected mice, blood transplantation revealed the presence of circulating long-term competitive repopulating HSCs after 2 days of clo-lip administration (Figure 5C), with multilineage engraftment in 5 of 6 recipients (Fisher exact test; $P = .008$), and after 4 days of clo-lip, multilineage engraftment was observed in 7 of 7 recipients (Fisher exact test; $P = .0006$). Blood chimerism from mice mobilized with clo-lip for 4 days was 90% in recipients,

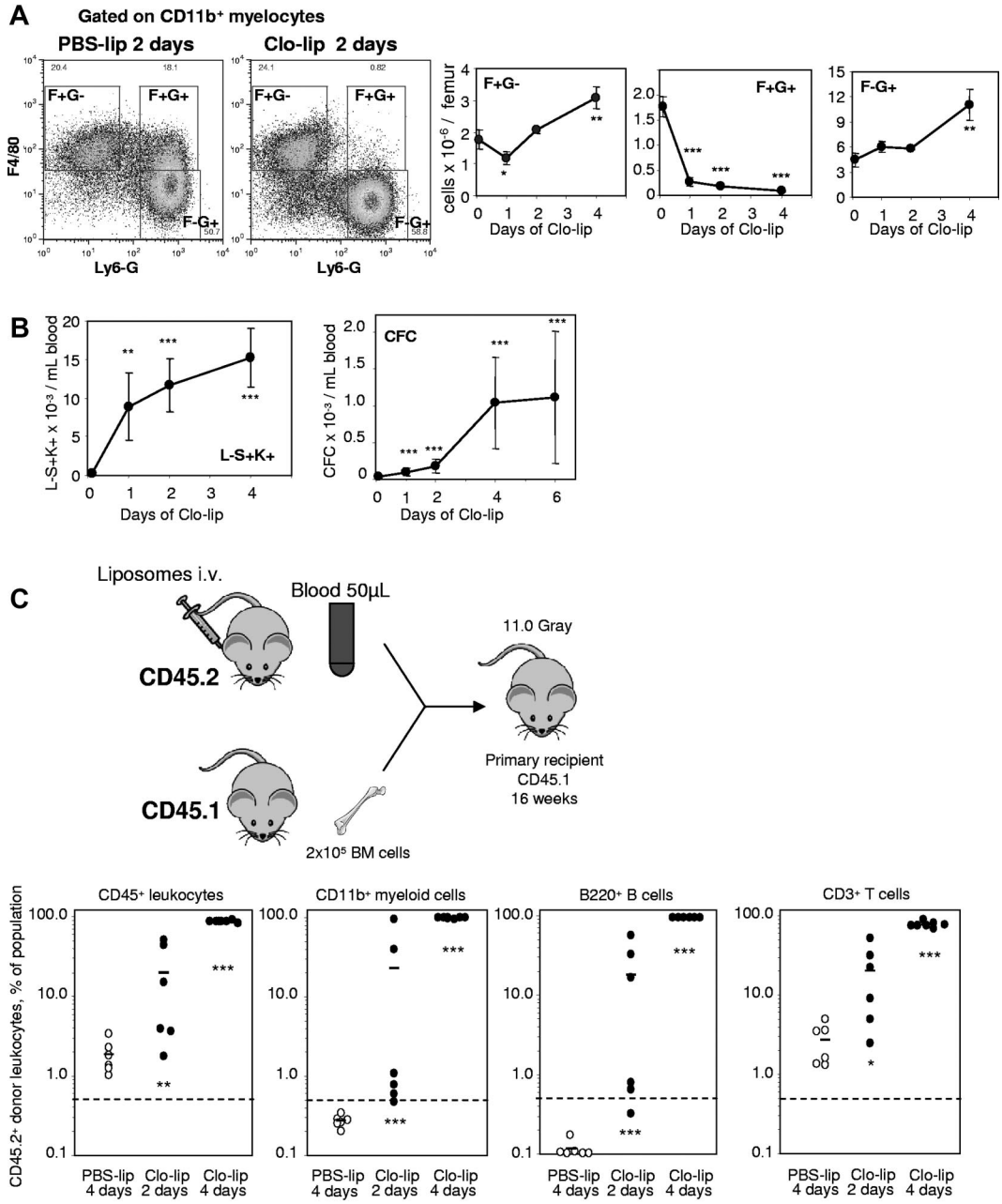

Figure 5. In vivo depletion of macrophages with clodronate-loaded liposomes mobilizes HSCs. (A) Effect of a 2-day treatment with clo-lip and PBS-lip on the number of BM F4/80$^+$Ly-6G$^-$CD11b$^+$ (F^+G^-), F4/80$^+$Ly-6G$^+$CD11b$^+$ (F^+G^+) macrophages and F4/80$^-$Ly-6G$^+$CD11b$^+$ (F^-G^+) granulocytes measured by flow cytometry. The 2 dot-plots illustrate the loss of F^+G^+. Data are mean ± SD of 4 mice per group. (B) Effect of liposomes on the number of circulating Lin$^-$Sca1$^+$KIT$^+$ HSPCs and CFCs. Data are mean ± SD of 4 mice per group. (C) Mobilization of long-term reconstituting HSCs in competitive repopulation assay. Test donor CD45.2$^+$ mice were injected with clo-lip for 2 or 4 days, or PBS-lip for 4 days. Next, 50 µL blood was transplanted in competition with 200 000 competing CD45.1$^+$ BM cells into lethally irradiated CD45.1$^+$ recipients. Donor CD45.2$^+$ contribution was measured in CD45$^+$ leukocytes, myeloid, B, and T cells 16 weeks after transplantation. Contribution was estimated to be positive when the proportion of CD45.2$^+$ donor cells was above 0.5% in each lineage. ***$P < .001$, **$P < .01$, and *$P < .05$ between PSB-lip– and clo-lip–treated mice.

compared with 29% ± 13% donor chimerism when donor mice were mobilized with G-CSF for 3 days (Figure 2H).

Administration of clo-lip also dramatically down-regulated osteocalcin, CXCL12, KL, and Ang-1 mRNA in the BM over 10-fold within 24 hours, reflecting a rapid disruption of niche function when BM phagocytic macrophages were ablated (Figure 6A). Immunohistochemistry showed a severe depletion of endosteal osteomacs in the secondary spongiosa of the metaphysis within 24 hours of clo-lip administration (Figure 6B) and flattened morphology of osteocalcin-positive osteoblasts, followed by osteoblast depletion at day 2 of clo-lip administration (Figure 6B). This time course of depletion in osteoblast number, and bone formation after clo-lip administration, was confirmed by histomorphometry (Figure 6C). TRAP staining and histomorphometry also confirmed a decrease in osteoclast number and function within 2 days of clo-lip administration (supplemental Figure 3).

Loss of osteoblasts with clo-lip treatment is not mediated by mature granulocytes or their proteases

Granulocytes can release proteases, such as NE, catG, and matrix metalloproteinase (MMP)-9, which cleave and inactivate the

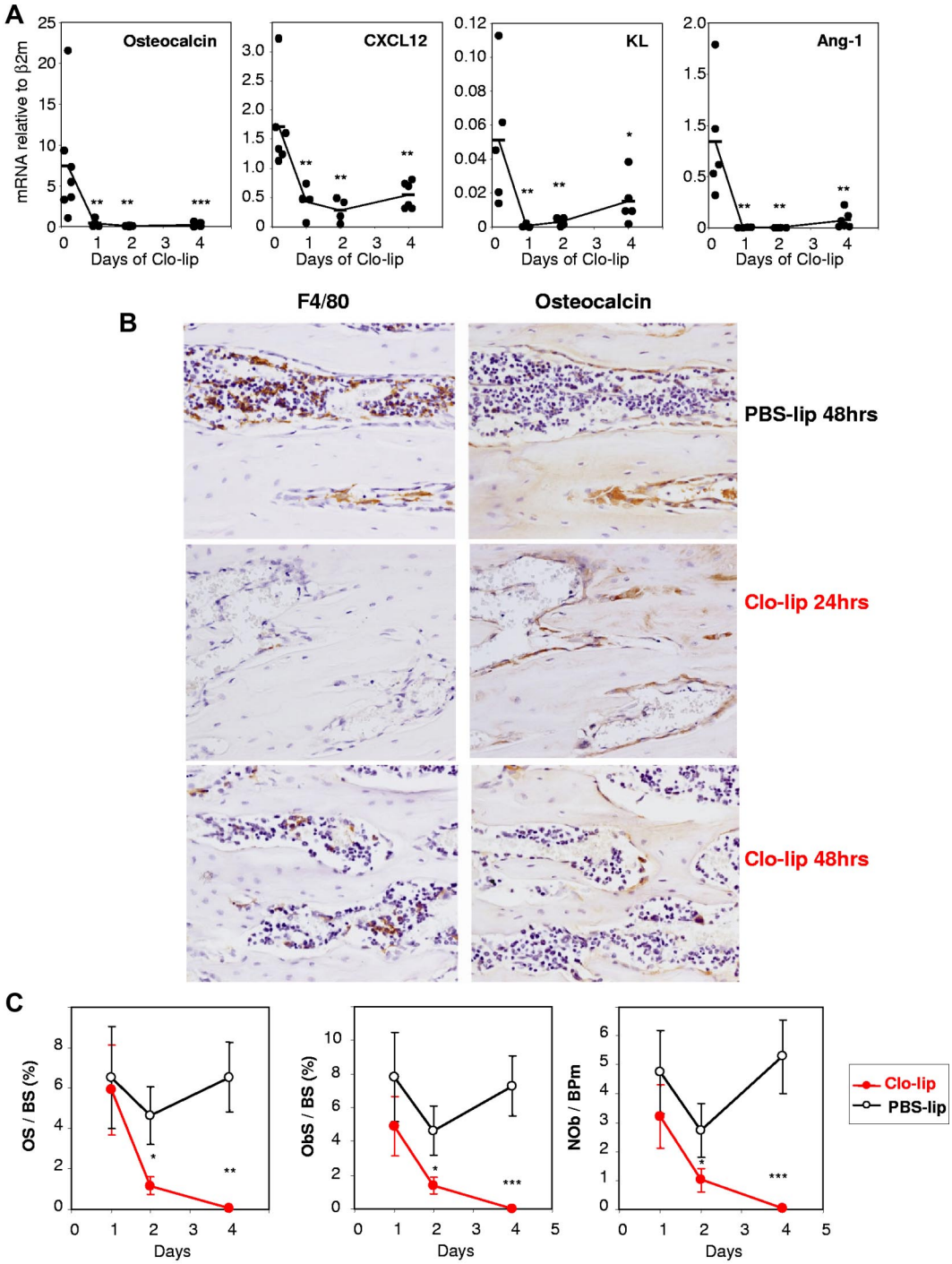

Figure 6. Effect of clodronate-loaded liposomes on endosteal niches. (A) Time course of clo-lipo treatment on mRNA expression of osteocalcin, CXCL12, KL, and Ang-1 in endosteal cells relative to β2-microglobulin. Each symbol represents 1 mouse, and bars are average for each group. ***$P < .001$, **$P < .01$, and *$P < .05$ between PSB-lip–(time 0) and clo-lip–treated mice. (B) Immunohistochemical staining of femoral sections from C57BL/6 mice treated with clo-lip (24 or 48 hours) or PBS-lip (48 hours). Brown positive staining for F4/80 and osteocalcin is shown in near serial sections of metaphysal bone. Clo-lip treatment resulted in the depletion of F4/80$^+$ cells at 24 and 48 hours after clo-lip treatment. Subsequent reduction in osteocalcin$^+$ osteoblasts occurred at 48 hours. All sections were counterstained with hematoxylin. Original magnification ×20. (C) Histomorphometry for osteoid surface per bone surface (OS/BS), osteoblast surface per bone surface (ObS/BS), and number of osteoblasts per bone perimeter (NOb/BPm) in the trabeculae of the proximal tibial secondary spongiosa from mice treated with clo-lip or PBS-lip. Data are means ± SEM of both tibias from 4-8 mice per group. *$P < .05$, **$P < .01$; and ***$P < .001$.

interactions maintaining HSPCs within the BM, thereby initiating mobilization.[20,29,41,42] As 4 days of clo-lip treatment would lead to an increase in Ly-6G$^+$F4/80$^-$CD11b$^+$ granulocytic-lineage cells in the BM (Figure 5A), we assessed neutrophil proteases in BM fluids during clo-lip treatment. No increase in activity or concentration of these proteases was observed in BM fluids from clo-lip–treated mice (Figure 7A-B) when osteoblast depletion (Figure 6B-C), decreased transcription of HSC–trophic cytokines/chemokines/adhesive factors (Figure 6A), and mobilization of CFCs, Lin$^-$Sca1$^+$KIT$^+$ HSPCs, and LT-CRCs had commenced (Figure 5). At day 4 of clo-lip treatment, catG and MMP-9 concentrations were slightly increased (Figure 6A-B) in synchrony with the late

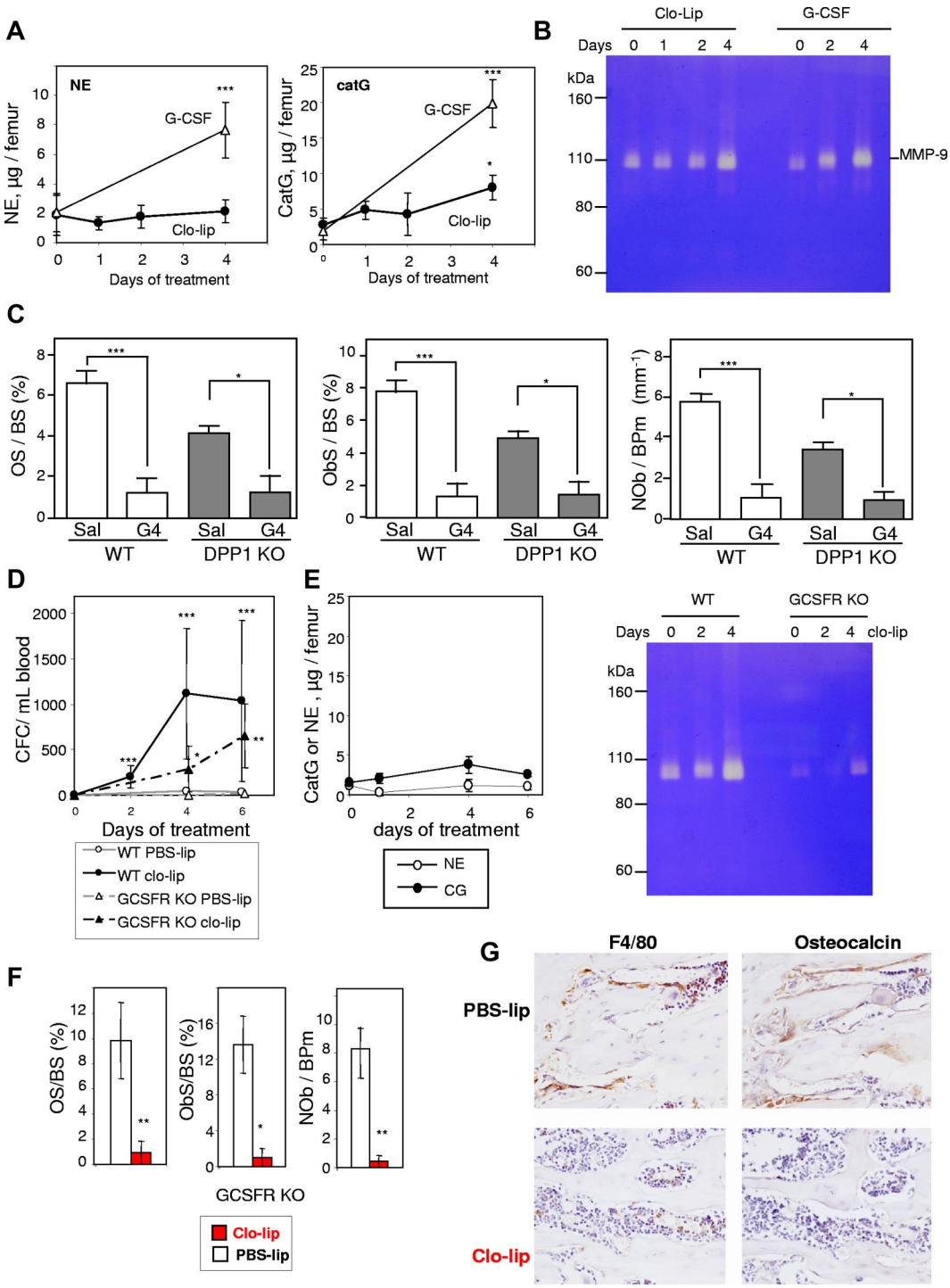

Figure 7. Mobilization with clo-lip is independent of neutrophil proteases. (A) Concentration of proteolytically active NE and catG in BM fluids from clo-lip–treated C57BL/6 mice. Results are compared with 129Sv mice treated for 4 days with G-CSF (4 mice per time point; mean ± SD). (B) Gelatin zymography of BM fluids from C57BL/6 mice treated with clo-lip or G-CSF. Each lane contains a pool of BM fluids from 4 different mice. (C) Effect of G-CSF on osteoid surface per bone surface (OS/BS), osteoblast surface per bone surface (ObS/BS), and number of osteoblasts per bone perimeter (NOb/BPm) in DPP1-deficient mice. Data are means ± SEM of both tibias from 4 mice per group. Effect of clo-lip in GCSFR-deficient mice on mobilization of CFC in blood (D) and (E) concentrations of active NE, catG, and MMP-9 in BM fluids (4 mice per time point; mean ± SD). Effect of 4-day clo-lip treatment on osteoid surface per bone surface (OS/BS), osteoblast surface per bone surface (ObS/BS), number of osteoblasts per bone perimeter (NOb/BPm) (F), osteocalcin$^+$ mature osteoblasts (G, right panels, metaphyseal trabecular bone), and F4/80$^+$ osteomacs (G, left panels) in *GCSFR* knockout mice (means ± SEM and representative ×40 magnification images, respectively, 3 mice per group). *$P < .05$, **$P < .01$, and ***$P < .001$.

expansion of Ly-6G$^+$ granulocytic cells in the BM (Figure 5A) and increased HSPC mobilization (Figure 5B-C). The absence of significant BM protease activity during the first 2 days of clo-lip administration suggests that the release of NE, catG, and MMP-9 in the BM is not the primary factor inhibiting osteoblast function in response to clo-lip.

In addition, a reduction in osteoid surface and osteoblast number in response to G-CSF in DPP1-deficient mice, which

mobilize normally in response to G-CSF, despite the complete absence of active NE and catG,[43] confirmed that NE and catG are not necessary for osteoblast inhibition in response to G-CSF (Figure 7C).

Finally, using GCSFR KO mice, which have very few functional granulocytes and almost no neutrophil protease activity (Figure 7E), clo-lip administration still elicited HSPC mobilization (Figure 7D) concomitant with osteoblast and osteomac depletion (Figure 7F-G). Altogether, these data show that CFC mobilization and loss of osteoblasts in response to macrophage depletion or G-CSF treatment is not initiated by proteases released from mature granulocytes in the BM.

Discussion

Cells of the osteoblast lineage are essential for the maintenance of HSCs in the BM,[8-12] producing cytokines, chemokines, and cell-adhesion molecules that regulate HSC fate, including CXCL12, KL, Ang-1, and osteopontin. G-CSF administration transiently suppressed these cells, leading to pronounced decreases in bone formation and mineralization at the endosteum and reduced expression of CXCL12, KL, and Ang-1 in the BM. This inhibition of endosteal niches coincided with the mobilization of HSC and was not mediated by osteoclasts, but by a loss of osteoblast-supportive osteomacs and/or other phagocytic macrophages with an unusual F4/80$^+$Ly-6G$^+$CD11b$^+$ phenotype. Indeed, in vivo depletion of macrophages in 2 mechanistically unrelated models depleted osteoblasts and HSC niche function, causing robust HSPC mobilization into the blood. These data demonstrate that BM macrophages play a critical role in the maintenance of endosteal HSC niches in vivo.

Since osteoblasts do not express G-CSFR, the mechanisms of G-CSF–mediated osteoblast suppression must be indirect,[16,23] and several mediators have been proposed. Although adrenergic receptors are involved in HSPC mobilization in response to G-CSF,[16] they are clearly not the only players. In mice knocked out for both β2 and β3 adrenergic receptors, HSPC mobilization in response to G-CSF was reduced by only 50%.[44] Furthermore, treatment with the β adrenergic antagonist propanolol in WT adult mice reduced G-CSF–induced HSPC mobilization by only 30%.[16] BM leukocytes also play an important role in osteoblast regulation. Indeed, in *G-CSFR* knockout to wild-type transplantation chimeras, where nerve and BM stromal cells express G-CSFR but donor BM leukocytes do not, CFCs are no longer mobilized in response to G-CSF nor are osteoblasts suppressed.[17] Therefore, BM leukocytes are critical to both endosteal osteoblast suppression and HSPC mobilization.

Osteoclasts have also been reported to play a role in HSPC mobilization by secreting cathepsin K, which cleaves and inactivates CXCL12 and KL.[45] These conclusions were drawn from experiments at a single time point of G-CSF mobilization. However, our data clearly demonstrate that neither osteoclast number nor cathepsin K transcription is increased during the initiation of G-CSF–mediated HSC mobilization. In fact, a rise in osteoclasts and cathepsin K occurs subsequently when mobilization is over (herein and Takamatsu et al[15]). Furthermore, osteoclast inhibition with the potent bisphosphonate zoledronate did not inhibit, but enhanced, mobilization of CFCs and competitive repopulating cells. We now have congruent data from 2 inbred mouse strains demonstrating that: (1) osteoclast numbers and bone degradation increase only after cessation of G-CSF treatment and (2) that bisphosphonates (zoledronate or pamidronate[15]) synergize with G-CSF to increase CFC mobilization. In addition, in the 2 macrophage-depletion models used here, osteoclast numbers were reduced as a result of the depletion strategies, yet robust HSC mobilization occurred. Hence, we conclude that osteoclasts and release of cathepsin K are not the prime initiators of osteoblast suppression and HSC mobilization in response to G-CSF.

Tissue macrophages are phenotypically and functionally diverse, and some subpopulations have trophic roles specific to their resident tissue, particularly in tissue development[46] and wound healing.[47] BM contains at least 2 trophic resident macrophage populations: central BM macrophages and endosteal osteomacs.[26] Central BM macrophages are located throughout the BM stroma and often cluster with erythroid precursors to support erythropoiesis.[48] More recently, we described osteomacs, which support osteoblast function and maintain bone-forming surfaces in vivo.[26] We now provide evidence that BM macrophage populations are also essential for the maintenance of the endosteal HSC niche. Furthermore, their depletion results in loss of endosteal osteoblasts, down-regulation of CXCL12, KL, and Ang-1 mRNA at the endosteum, and mobilization of HSPC into the blood.

After administration of G-CSF, we found that osteomacs vacate endosteal surfaces as early as days 1-2 after treatment, paralleling or even preceding endosteal osteoblast depletion. This sequence of events observed in mice administered G-CSF almost exactly phenocopies that observed during macrophage depletion by either ligand-treated Mafia transgenic mice or clo-lip administration in wild-type mice. In particular, during clo-lip treatment, the disappearance of osteomacs at endosteal bone surfaces and of over 95% of F4/80$^+$Ly-6G$^+$CD11b$^+$ phagocytic macrophages coincided with the initiation of HSPC mobilization into the blood. At this time, endosteal osteoblasts persisted on endosteal surfaces, although a marked drop in mRNA for HSC-trophic cytokines confirmed that osteoblast function was already compromised. Of note, the chain of events following clo-lip administration was not dependent on mature granulocytes or on the release of proteases NE, catG, or MMP-9 in the BM. Indeed, Clo-lip induced HSPC mobilization, osteomac loss and inhibition of osteoblast function even in *GCSFR* knockout mice, despite few mature granulocytes and extremely low protease levels in the BM. Furthermore, in the Mafia model, granulocytes and macrophages were both ablated, but HSPCs were still mobilized. Therefore, granulocytes and their proteases were unlikely to be the primary drivers of osteoblast depletion and HSPC mobilization following macrophage depletion. This does not exclude the possibility that granulocytes subsequently amplified the mobilization response, as suggested by increased mobilization at day 4 of clo-lip treatment when F4/80$^-$Ly-6G$^+$CD11b$^+$ granulocytes accumulated in the BM. Our data are consistent with a recent abstract showing that activation of G-CSF signaling in *CD68*-expressing monocytes/macrophages alone in *GCSFR* knockout mice, which are neutropenic, is sufficient to elicit HSPC mobilization.[49]

In conclusion, we show that BM macrophages are required for the maintenance of HSC niches. Loss of these macrophages initiates a cellular cascade that ultimately collapses this trophic niche environment through loss of endosteal osteoblasts and subsequently egress of HSPC into the blood. While anatomic location of osteomacs within the endosteal niche supports the notion that this population of BM macrophages are HSC-niche

supportive, definitive dissection of the role of osteomacs versus central BM phagocytic macrophages is required. The mechanisms by which macrophages regulate HSC niches and whether they themselves directly interact with HSCs are currently under investigation.

Acknowledgments

We thank R. Wadley for the cell sorting and Dr L. Purton and Prof T. J. Martin for their insightful discussions.

This work was supported by grants 288701, 434515 (J.-P.L. and I.G.W.), 455941 (A.R.P. and L.J.R.), and 345401 (N.A.S.) from the National Health and Medical Research Council, Australia (NHMRC). I.G.W., N.A.S., A.R.P., and F.H. are Research Fellows of the NHMRC. J.-P.L. is a Senior Research Fellow of the Cancer Council of Queensland.

Authorship

Contribution: I.G.W., N.A.S., and A.R.P. planned and performed experiments, interpreted results, and wrote and edited the manuscript; V.B., B.N., F.H., I.J.P., and K.A.A. performed experiments and analyzed data; N.V.R. provided essential reagents and expertise; L.J.R. coconceived the work, planned, and performed experiments, interpreted results, and wrote and edited the manuscript; and J.-P.L. conceived and coordinated the work, planned and performed experiments, interpreted results, and wrote and edited the manuscript.

Conflict-of-interest disclosure: The authors declare no competing financial interests.

Correspondence: Jean-Pierre Lévesque, Hematopoietic Stem Cell Laboratory, Mater Medical Research Institute, Aubigny Place, Raymond Terrace, South Brisbane, QLD 4101, Australia; e-mail: jplevesque@mmri.mater.org.au.

References

1. Schofield R. The relationship between the spleen colony-forming cell and the haemopoietic stem cell. *Blood Cells.* 1978;4(1-2):7-25.
2. Arai F, Hirao A, Ohmura M, et al. Tie2/angiopoietin-1 signaling regulates hematopoietic stem cell quiescence in the bone marrow niche. *Cell.* 2004; 118(2):149-161.
3. Xie Y, Yin T, Wiegraebe W, et al. Detection of functional haematopoietic stem cell niche using real-time imaging. *Nature.* 2009;457(7225):97-101.
4. Kohler A, Schmithorst V, Filippi M-D, et al. Altered cellular dynamics and endosteal location of aged early hematopoietic progenitor cells revealed by time-lapse intravital imaging in long bones. *Blood.* 2009;114(2):290-298.
5. Lo Celso C, Fleming HE, Wu JW, et al. Live-animal tracking of individual haematopoietic stem/progenitor cells in their niche. *Nature.* 2009; 457(7225):92-97.
6. Winkler IG, Barbier V, Wadley R, Zannettino ACW, Williams S, Lévesque J-P. Positioning of bone marrow hematopoietic and stromal cells relative to blood flow in vivo: serially reconstituting hematopoietic stem cells reside in distinct nonperfused niches. *Blood.* 2010;116(3):375-385.
7. Grassinger J, Haylock DN, Williams B, Olsen GH, Nilsson SK. Phenotypically identical hemopoietic stem cells isolated from different regions of bone marrow have different biological potential. *Blood.* 2010;116(17):3185-3196.
8. Calvi LM, Adams GB, Weibrecht KW, et al. Osteoblastic cells regulate the haematopoietic stem cell niche. *Nature.* 2003;425(6960):841-846.
9. Zhang J, Niu C, Ye L, et al. Identification of the haematopoietic stem cell niche and control of the niche size. *Nature.* 2003;425(6960):836-841.
10. Visnjic D, Kalajzic Z, Rowe DW, Katavic V, Lorenzo J, Aguila HL. Hematopoiesis is severely altered in mice with an induced osteoblast deficiency. *Blood.* 2004;103(9):3258-3264.
11. Raaijmakers MHGP, Mukherjee S, Guo S, et al. Bone progenitor dysfunction induces myelodysplasia and secondary leukaemia. *Nature.* 2010; 464(7290):852-857.
12. Askmyr M, Sims NA, Martin TJ, Purton LE. What is the true nature of the osteoblastic hematopoietic stem cell niche? *Trends Endocrinol Metab.* 2009;20(6):303-309.
13. Nervi B, Link DC, DiPersio JF. Cytokines and hematopoietic stem cell mobilization. *J Cell Biochem.* 2006;99(3):690-705.
14. Lévesque JP, Winkler IG. Mobilization of hematopoietic stem cells: state of the art. *Curr Opin Organ Transpl.* 2008;13(1):53-58.
15. Takamatsu Y, Simmons PJ, Moore RJ, Morris HA, To LB, Lévesque JP. Osteoclast-mediated bone resorption is stimulated during short-term administration of granulocyte colony-stimulating factor but is not responsible for hematopoietic progenitor cell mobilization. *Blood.* 1998;92(9):3465-3473.
16. Katayama Y, Battista M, Kao WM, et al. Signals from the sympathetic nervous system regulate hematopoietic stem cell egress from bone marrow. *Cell.* 2006;124(2):407-421.
17. Christopher MJ, Link DC. Granulocyte colony-stimulating factor induces osteoblast apoptosis and inhibits osteoblast differentiation. *J Bone Min Res.* 2008;23(11):1765-1774.
18. Burnett SH, Beus BJ, Avdiushko R, Qualls J, Kaplan AM, Cohen DA. Development of peritoneal adhesions in macrophage depleted mice. *J Surg Res.* 2006;131(2):296-301.
19. Van Rooijen N, Sanders A. Liposome-mediated depletion of macrophages: mechanism of action, preparation of liposomes, and applications. *J Immunol Methods.* 1994;174(1-2):83-93.
20. Lévesque JP, Hendy J, Winkler IG, Takamatsu Y, Simmons PJ. Granulocyte colony-stimulating factor induces the release in the bone marrow of proteases that cleave c-KIT receptor (CD117) from the surface of hematopoietic progenitor cells. *Exp Hematol.* 2003;31(2):109-117.
21. Lévesque J-P, Winkler IG, Hendy J, et al. Hematopoietic progenitor cell mobilization results in hypoxia with increased hypoxia-inducible transcription factor-1α and vascular endothelial growth factor A in bone marrow. *Stem Cells.* 2007;25(8):1954-1965.
22. Sims NA, Brennan K, Spaliviero J, Handelsman DJ, Seibel MJ. Perinatal testosterone surge is required for normal adult bone size but not for normal bone remodeling. *Am J Physiol Endocrinol Metab.* 2006; 290(3):E456-E462.
23. Semerad CL, Christopher MJ, Liu F, et al. G-CSF potently inhibits osteoblast activity and CXCL12 mRNA expression in the bone marrow. *Blood.* 2005;106(9):3020-3027.
24. Lundberg P, Allison SJ, Lee NJ, et al. Greater bone formation of Y2 knockout mice is associated with increased osteoprogenitor numbers and altered Y1 receptor expression. *J Biol Chem.* 2007; 282(26):19082-19091.
25. Short BJ, Brouard N, Simmons PJ. Prospective isolation of mesenchymal stem cells from mouse compact bone. *Methods Mol Biol.* 2009;482: 259-268.
26. Chang MK, Raggatt L-J, Alexander KA, et al. Osteal tissue macrophages are intercalated throughout human and mouse bone lining tissues and regulate osteoblast function in vitro and in vivo. *J Immunol.* 2008;181(2):1232-1244.
27. Wu CA, Pettit AR, Toulson S, Grondahl L, Mackie EJ, Cassady AI. Responses in vivo to purified poly(3-hydroxybutyrate-co-3-hydroxyvalerate) implanted in a murine tibial defect model. *J Biomed Mater Res A.* 2009;91(3):845-854.
28. Lévesque JP, Hendy J, Takamatsu Y, Williams B, Winkler IG, Simmons PJ. Mobilization by either cyclophosphamide or granulocyte colony-stimulating factor transforms the bone marrow into a highly proteolytic environment. *Exp Hematol.* 2002;30(5):440-449.
29. Lévesque JP, Takamatsu Y, Nilsson SK, Haylock DN, Simmons PJ. Vascular cell adhesion molecule-1 (CD106) is cleaved by neutrophil proteases in the bone marrow following hematopoietic progenitor cell mobilization by granulocyte colony-stimulating factor. *Blood.* 2001;98(5): 1289-1297.
30. Kiel MJ, Yilmaz OH, Iwashita T, Yilmaz OH, Terhorst C, Morrison SJ. SLAM family receptors distinguish hematopoietic stem and progenitor cells and reveal endothelial niches for stem cells. *Cell.* 2005;121(7):1109-1121.
31. Komori T, Yagi H, Nomura S, et al. Targeted disruption of Cbfa1 results in a complete lack of bone formation owing to maturational arrest of osteoblasts. *Cell.* 1997;89(5):755-764.
32. Nakashima K, Zhou X, Kunkel G, et al. The novel zinc finger–containing transcription factor osterix is required for osteoblast differentiation and bone formation. *Cell.* 2002;108(1):17-29.
33. Liu F, Woitge HW, Braut A, et al. Expression and activity of osteoblast-targeted Cre recombinase transgenes in murine skeletal tissues. *Int J Dev Biol.* 2004;48(7):645-653.
34. Foudi A, Jarrier P, Zhang Y, et al. Reduced retention of radioprotective hematopoietic cells within the bone marrow microenvironment in CXCR4$-/-$ chimeric mice. *Blood.* 2006;107(6): 2243-2251.
35. Sugiyama T, Kohara H, Noda M, Nagasawa T. Maintenance of the hematopoietic stem cell pool by CXCL12-CXCR4 chemokine signaling in bone marrow stromal cell niches. *Immunity.* 2006; 25(6):977-988.
36. Lataillade JJ, Clay D, Bourin P, et al. Stromal

cell–derived factor 1 regulates primitive hematopoiesis by suppressing apoptosis and by promoting G0/G1 transition in CD34+ cells: evidence for an autocrine/paracrine mechanism. *Blood.* 2002; 99(4):1117-1129.

37. Mundy GR, Yoneda T, Hiraga T. Preclinical studies with zoledronic acid and other bisphosphonates: impact on the bone microenvironment. *Semin Oncol.* 2001;28(2 suppl 6):35-44.
38. Sudhoff H, Jung JY, Ebmeyer J, Faddis BT, Hildmann H, Chole RA. Zoledronic acid inhibits osteoclastogenesis in vitro and in a mouse model of inflammatory osteolysis. *Ann Otol Rhinol Laryngol.* 2003;112(9 Pt 1):780-786.
39. Rehli M, Sulzbacher S, Pape S, et al. Transcription factor Tfec contributes to the IL-4-inducible expression of a small group of genes in mouse macrophages including the granulocyte colony-stimulating factor receptor. *J Immunol.* 2005; 174(11):7111-7122.
40. Verstegen MM, van Hennik PB, Terpstra W, et al. Transplantation of human umbilical cord blood cells in macrophage-depleted SCID mice: evidence for accessory cell involvement in expansion of immature CD34+CD38− cells. *Blood.* 1998;91(6):1966-1976.
41. Lévesque JP, Hendy J, Takamatsu Y, Simmons PJ, Bendall LJ. Disruption of the CXCR4/CXCL12 chemotactic interaction during hematopoietic stem cell mobilization induced by GCSF or cyclophosphamide. *J Clin Invest.* 2003;111(2): 187-196.
42. Heissig B, Hattori K, Dias S, et al. Recruitment of stem and progenitor cells from the bone marrow niche requires MMP-9–mediated release of kit-ligand. *Cell.* 2002;109(5):625-637.
43. Lévesque JP, Liu F, Simmons PJ, et al. Characterization of hematopoietic progenitor mobilization in protease-deficient mice. *Blood.* 2004; 104(1):65-72.
44. Mendez-Ferrer S, Battista M, Frenette PS. Cooperation of beta(2)- and beta(3)-adrenergic receptors in hematopoietic progenitor cell mobilization. *Ann N Y Acad Sci.* 2010;1192(1):139-144.
45. Kollet O, Dar A, Shivtiel S, et al. Osteoclasts degrade endosteal components and promote mobilization of hematopoietic progenitor cells. *Nat Med.* 2006;12(6):657-664.
46. Pollard JW. Trophic macrophages in development and disease. *Nat Rev Immunol.* 2009;9(4):259-270.
47. Bryer SC, Fantuzzi G, Van Rooijen N, Koh TJ. Urokinase-type plasminogen activator plays essential roles in macrophage chemotaxis and skeletal muscle regeneration. *J Immunol.* 2008; 180(2):1179-1188.
48. Mohandas N, Prenant M. Three-dimensional model of bone marrow. *Blood.* 1978;51(4): 633-643.
49. Rao M, Christopher M, Woloszynek J, Liu F, Link DC. Expression of the G-CSF receptor in monocytes is sufficient to mediate osteoblast suppression and HSPC mobilization by G-CSF in mice [abstract]. *Blood.* 2009;114(22):563.